Journal of Power Sources 196 (2011) 6274–6283

Contents lists available at ScienceDirect

Journal of Power Sources

journal homepage: www.elsevier.com/locate/jpowsour

PEMFC contamination model: Foreign cation exchange with ionomer protons

Jean St-Pierre*

University of South Carolina, Department of Chemical Engineering, 301 Main Street, Columbia, SC 29208, USA

ARTICLE INFO

Article history:
Received 23 January 2011
Received in revised form 4 April 2011
Accepted 4 April 2011
Available online 8 April 2011

Keywords:
Contamination
Foreign cation
Ion exchange
Ionomer
Proton exchange membrane fuel cell

ABSTRACT

A generic, transient fuel cell ohmic loss mathematical model was developed for the case of contaminants that ion exchange with ionomer protons. The model was derived using step changes in contaminant concentration, constant operating conditions and foreign cation transport via liquid water droplets. In addition, the effect of ionomer cations redistribution within the ionomer on thermodynamic, kinetic and mass transport losses and migration were neglected. Thus, a simpler, ideal, ohmic loss case is defined and is applicable to uncharged contaminant species and gas phase contaminants. The closed form solutions were validated using contamination data from a membrane exposed to NH_3. The model needs to be validated against contamination and recovery data sets including an NH_4^+ contaminated membrane exposed to a water stream. A method is proposed to determine model parameters and relies on the prior knowledge of the initial ionomer resistivity. The model expands the number of previously derived cases. Most models in this inventory, derived with the assumption that the reactant is absent, lead to different dimensionless current vs. time behaviors similar to a fingerprint. These model characteristics facilitate contaminant mechanism identification. Separation between membrane and catalyst (electroinactive contaminant) contamination is conceivably possible using additional indicative cell resistance measurements. Contamination is predicted to be significantly more severe under low relative humidity conditions.

1. Introduction

Proton exchange membrane fuel cells (PEMFCs), an alternative power source currently being developed [1], is sensitive to contaminants present in reactant streams and released from system components [2]. Generic models were developed to address the large number of existing and unidentified contaminants [3–6]. Such models are useful to classify contaminants (mechanism identification), set tolerance limits and design experimental procedures for validation and extraction of model parameters. For instance, fuel cell testing with low contaminant concentrations requires significant time and resources because effects are small and not easily measured with certainty. A simple model for membrane contamination has not yet been derived and is needed to complete the existing library.

Several models have already been proposed showing that all types of performance losses take place within a contaminated PEMFC including thermodynamic, kinetic, ohmic and mass transport losses [7–13]. Experimental data support this statement [14]. However, in most model cases, the physics associated with the ion exchange process were not taken into account [7–12]. Langmuir isotherms were recently used [13] but such an approach was discontinued to characterize ion exchangers [15] because it does not reproduce their behavior.

A simple transient PEMFC contamination model is derived using a similar approach as prior efforts [3–6] with a focus on the membrane ion exchange with foreign cations. The approach considers first order effects, to maintain model generality and applicability to many different cations, and the derivation of an analytical solution, to simplify its use for predictions, validation and extraction of model parameters.

2. Model assumptions

Fig. 1a illustrates the path taken by a foreign cation X^{+n} from the flow field channel to the ionomer exchange site. It is assumed that liquid water droplets maintain a steady flow and concentration of foreign cations originating from the environment or system components. Liquid water is not necessarily required to introduce foreign cations into the fuel cell. Particles containing soluble salts and entrained by the reactant flow provide a supply of foreign cations by dissolution in fuel cell areas containing water droplets. The presence of product water in the gas diffusion electrode creates a path for the foreign cations to reach the ionomer by diffusion. The

* Present address: Hawaii Natural Energy Institute, School of Ocean and Earth Science and Technology, University of Hawaii – Manoa, 1680 East-West Road, Honolulu, HI 96822, USA. Tel.: +1 808 956 3909; fax: +1 808 956 2336.
E-mail address: jsp7@hawaii.edu

0378-7753/$ – see front matter © 2011 Elsevier B.V. All rights reserved.
doi:10.1016/j.jpowsour.2011.04.008

Nomenclature

a	empirical Eqs. (16) and (17) parameter (respectively Ω^{-1} cm^{-1} and dimensionless)
A	membrane surface area (cm^2)
b	empirical Eqs. (16) and (17) parameter (respectively Ω^{-1} cm^{-1} and dimensionless) or Tafel slope (V)
c_g	foreign contaminant concentration in the gas phase (mol cm^{-3})
c_i	equivalent ionic concentration in the ionomer phase (mol cm^{-3})
c_{i,H^+}	proton concentration in the ionomer phase (mol cm^{-3})
$c_{i,X^{+n}}$	foreign cation concentration in the ionomer phase (mol cm^{-3})
c_l	equivalent ionic concentration in the liquid phase (mol cm^{-3})
c_{l,H^+}	proton concentration in the liquid phase (mol cm^{-3})
$c_{l,X^{+n}}$	foreign cation concentration in the liquid phase (mol cm^{-3})
c_R	reactant concentration (mol cm^{-3})
d	distance (cm)
d_g	gas phase boundary layer thickness (cm)
d_i	ionomer phase thickness (cm)
d_l	liquid phase thickness (cm)
D_g	diffusion coefficient in the gas phase (cm^2 s^{-1})
D_i	diffusion coefficient in the ionomer phase (cm^2 s^{-1})
D_l	diffusion coefficient in the liquid phase (cm^2 s^{-1})
e	polarization curve parameter characterizing mass transport effects (V)
E	cell potential (V)
E_a	anode potential (V)
E_c	cathode potential (V)
E_0	polarization curve constant cell potential parameter (V)
Est_m	experimental estimates for specific model parameters (m is an integer with a value of 1–4)
f	polarization curve parameter characterizing mass transport effects (cm^2 A^{-1})
i	current density (A cm^{-2})
i_X	current density associated with a contaminant X (A cm^{-2})
$i_{X^{+n}}$	current density associated with a contaminant X^{+n} (A cm^{-2})
n	foreign cation charge
N	proton flux in the liquid phase (mol s^{-1} cm^{-2})
$Pé$	Péclet number
R	areal membrane resistance (Ω cm^2)
t	time (s)
$t_{0.5}$	time required for the dimensionless current to decrease to a value equal to half the difference between initial and steady state values (s)
u	liquid phase velocity (cm s^{-1})
V	ionomer volume (cm^3)
x	equivalent ion fraction in the liquid phase
x_{H^+}	equivalent proton fraction in the liquid phase
$x_{X^{+n}}$	equivalent foreign cation fraction in the liquid phase
y	equivalent ion fraction in the ionomer phase
y_{H^+}	equivalent proton fraction in the ionomer phase
$y_{X^{+n}}$	equivalent foreign cation fraction in the ionomer phase
$\alpha^{H^+}_{X^{+n}}$	separation factor
σ	ionomer conductivity (Ω^{-1} cm^{-1})

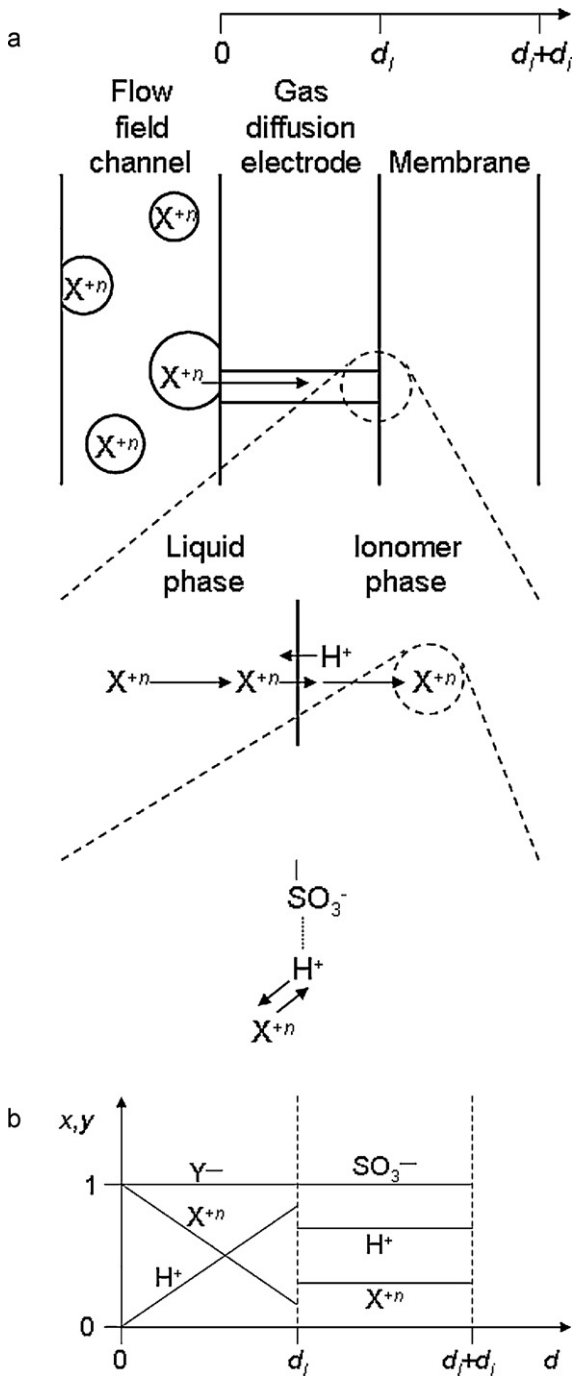

Fig. 1. Contaminant X^{+n} transport pathway towards the ionomer (a). Liquid phase transport in the flow field and the gas diffusion electrode is followed by penetration into the ionomer at its surface. Subsequently, X^{+n} diffuses towards an ion exchange site where it associates. Ion exchange stoichiometry is not taken into account in this schematic illustration. Equivalent ion fractions in both liquid and ionomer phases under liquid phase mass transport control after contamination initiation and before a steady state is reached (b). For the case illustrated, the foreign cation X^{+n} is preferred by the ionomer ($\alpha^{H^+}_{X^{+n}} < 1$ and $y_{X^{+n}} > x_{X^{+n}}$).

existence of such paths at preferential locations on the gas diffusion electrode was observed with in situ transparent cell designs and ex situ [16,17]. The path length is assumed to be of the same order as the electrode thickness (Fig. 1a). At the water/ionomer interface, the foreign cations easily enter the ionomer. This process is not rate determining for theoretical reasons and is supported by experimental data [15]. Subsequently, foreign cations move within the ionomer bulk by diffusion before associating themselves with

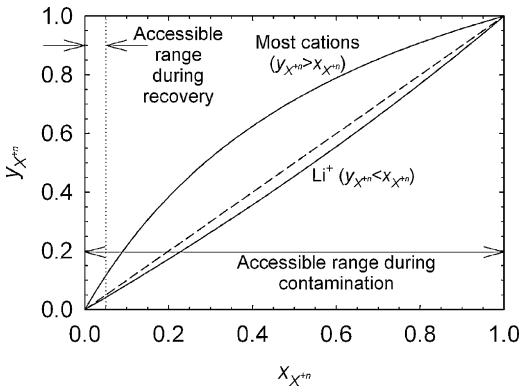

Fig. 2. Schematic ion exchange isotherms for the case of a foreign cation X^{+n} and H^+ (Nafion in contact with a dilute solution of XY_n). Accessible $x_{X^{+n}}$ range during contamination and recovery are also indicated. An isotherm of the form $y_{X^{+n}} = 1/[1 + \alpha^{H^+}_{X^{+n}}(1 - x_{X^{+n}})/x_{X^{+n}}]$ was used assuming equal cation charges and a constant selectivity coefficient thus reducing the expression to the separation factor definition [15,32]. For illustrative purposes, $\alpha^{H^+}_{X^{+n}} = 1.2$ for Li^+ whereas for other cations, $\alpha^{H^+}_{X^{+n}} = 0.4$.

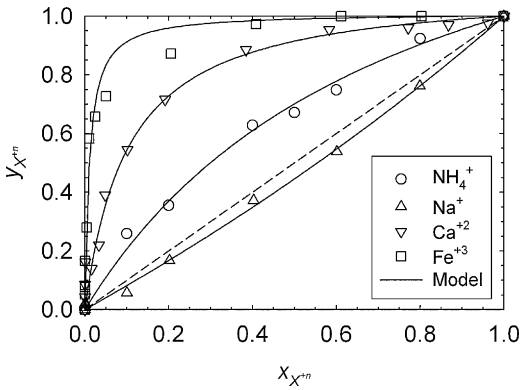

Fig. 3. Validation of the selected ion exchange isotherm ($y_{X^{+n}} = 1/[1 + \alpha^{H^+}_{X^{+n}}(1 - x_{X^{+n}})/x_{X^{+n}}]$) with different cations in Nafion 417 data [31]. Separation factors and correlation coefficients are given in Table 1.

exchange sites. This last step is not rate determining unless the exchange sites chelate foreign cations to form complexes [15]. The protons leaving the ionomer travel through the entire electrode thickness to compensate for the foreign cations flux towards the ionomer and maintain the charge balance (the anion concentration is constant, Fig. 1b).

Anions were not included in Fig. 1a because they are prevented from entering the ionomer owing to Donnan exclusion [15,18]. The presence of fixed negative charges (sulfonate sites) within the polymer ensures the absence of foreign anions for solutions with a concentration up to 0.1 N or more. Water production within fuel cells ensures that in most cases this limit is not exceeded unless a catastrophic event takes place (for example, flooding of the air intake by sea water). Therefore, it is assumed that the concentration of the foreign cation is relatively low (anions do not need to be considered). By contrast, Donnan exclusion is not always considered to explain the anion effect [19]. This statement does not imply that anions do not have any effect. For instance, the ionomer proton spills over the catalyst surface and diffuses on its surface thus enlarging the active area outside the ionomer [20–22]. The presence of a complexing anion dissolving the Pt would reduce the active area and increase the kinetic losses. Such kinetic losses are not considered here.

Foreign cations such as NH_4^+, Na^+, K^+, Rb^+, Cs^+, Ag^+, Ca^{2+}, Co^{2+}, Cu^{2+}, Ni^{2+}, Zn^{2+}, Fe^{3+} and Ce^{3+} are generally preferred by the Nafion ionomer over H^+ [12,23–31]. Only Li^+ appears to show a different behavior (H^+ is slightly preferred [12,27]) but this observation does not affect membrane contamination deductions. Representative ion exchange isotherms for these specific cases are depicted in Fig. 2 to discuss the extent of the foreign cation exchange with the ionomer proton. Other ions also need to be considered in the product water including the foreign anion Y^- and water dissociation products:

$$2H_2O \leftrightarrow H_3O^+ + OH^- \tag{1}$$

It is assumed that the foreign anion is not hydroxyl and, $X(OH)_n$ and HY are highly soluble. The equivalent foreign cation and proton ionic fractions are [15]:

$$x_{X^{+n}} = \frac{nc_{l,X^{+n}}}{nc_{l,X^{+n}} + c_{l,H^+}} = \frac{nc_{l,X^{+n}}}{c_l} \tag{2}$$

$$x_{H^+} = \frac{c_{l,H^+}}{nc_{l,X^{+n}} + c_{l,H^+}} = 1 - x_{X^{+n}} \tag{3}$$

During the contamination process, if $nc_{l,X^{+n}} >> c_{l,H^+}$ then $x_{X^{+n}} \approx 1$ and $y_{X^{+n}} \approx 1$ whereas if $nc_{l,X^{+n}} << c_{l,H^+}$ then $x_{X^{+n}} \approx 0$ and $y_{X^{+n}} \approx 0$ (Fig. 2). For other intermediate values of $x_{X^{+n}}$, generally $y_{X^{+n}} > x_{X^{+n}}$ (Fig. 2). In other words, it is assumed that the contaminant concentration may span the entire range (Fig. 2). Therefore, to minimize the membrane contamination extent, the foreign cation concentration needs to be significantly lower than the proton concentration in the product water (10^{-7} M at 25 °C). The situation during the recovery process is different because $nc_{l,X^{+n}} << c_{l,H^+}$, $x_{X^{+n}} \approx 0$ and $y_{X^{+n}} \approx 0$ (Fig. 2). In other words, few foreign cations are present near the ionomer. Thus, it is expected that a contaminated cell will recover most of its performance loss without adding any mitigation strategy if given sufficient time and contact with liquid water. The present discussion is extendable to other cases including other foreign anions (different species and ionic charges), existence of a common anion (OH^-), sparsely soluble components and the presence of CO_2 in air (pH change affecting Eqs. (2) and (3)):

$$CO_2 + 2H_2O \leftrightarrow HCO_3^- + H_3O^+ \tag{4}$$

The ion exchange isotherm is expressed by the separation factor [15]:

$$\alpha^{H^+}_{X^{+n}} = \frac{y_{H^+}x_{X^{+n}}}{y_{X^{+n}}x_{H^+}} = \frac{(1 - y_{X^{+n}})x_{X^{+n}}}{y_{X^{+n}}(1 - x_{X^{+n}})} \tag{5}$$

Eq. (5) leads to:

$$y_{X^{+n}} = \frac{1}{1 + (\alpha^{H^+}_{X^{+n}}(1 - x_{X^{+n}})/x_{X^{+n}})} \tag{6}$$

Eq. (6) should not be confused with the selectivity coefficient which is similar in form to a chemical equilibrium constant and includes stoichiometric coefficients arising in the ion exchange equilibrium due to unequal cation charges [15]. Eq. (6) corresponds to the selectivity coefficient assuming equal cation charges [15,32]. The selectivity coefficient only mimics the chemical equilibrium constant because ion exchange is not a chemical reaction (ions do not react but change phases). As a result, the selectivity coefficient is not constant [15] as opposed to a chemical equilibrium constant. Fig. 3 data indicate that Eq. (6) ion exchange isotherm accurately represents the behavior of an ionomer in the presence of different cations even if in several cases cations do not have equal charges. Adoption of Eq. (6) contributes to the development of a generic contamination model.

Foreign cations move in the product water by two different migration effects. The product water moving in gas diffusion electrode pores (Fig. 1a) is subjected to a potential gradient extending from the catalyst layer to the flow field channel. This potential gra-

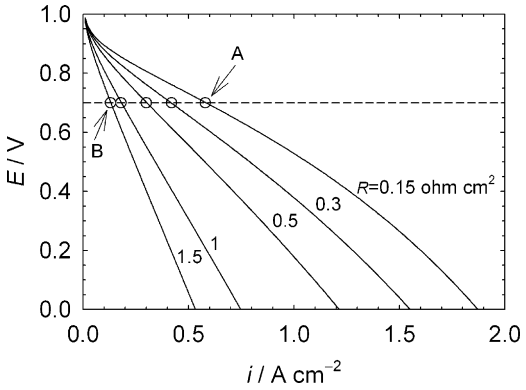

Fig. 4. Schematic polarization curves during the contamination process at constant cell potential. The operating points are located in the ohmic regime. The initial operating point gradually moves from point A to point B as the ionomer is contaminated with the foreign cation and the resistance increases. The polarization curves were generated using $E_0 - b\log(i) - Ri - e\exp(fi)$ with $E_0 = 0.95$ V, $b = 0.07$ V, $e = 0.1$ V, $f = 1$ cm^2 A^{-1} (R values are given in figure).

dient is small and typically less than 10–20 mV at ~1 A cm^{-2} [33,34] and thus is not considered an important model element because the water ionic resistivity is high and the resulting current is small. The contribution arising from the difference in cation mobility is not negligible (H^+, X^{+n}) and is assessable using liquid junction potential theory [35]. Cation migration in dilute solutions such as ground water is negligible because the contaminant ionic strength is much smaller than other ions [36] acting as a supporting electrolyte [35]. However, this assumption cannot be made here otherwise it would minimize the extent of contamination (Eq. (6)) by reducing the foreign cation equivalent ionic fraction (Eq. (2)). Ion migration is assumed to be negligible here for several reasons including consideration of relevant cases such as uncharged contaminant uptake by the ionomer affecting its conductivity, gas phase contaminants (Section 4.1) and accuracy determination of a simpler model. As already mentioned, the main objective is the development of an explicit analytical solution to the contamination model. Such an objective is not considered possible with the inclusion of migration effects. For instance, an analytical solution to the ion exchange problem is only possible for two cases [15] requiring restrictive assumptions such as absence of ionomer selectivity ($\alpha^{H^+}_{X+n} = 1$) and equal valence ions or equal counter ions mobility. Convection is also assumed to be negligible because the Péclet number $Pé = ud_l/D_l$ [37] is less than 1 ($u < 0.0005$ cm s^{-1} at 0.1 A cm^{-2} [38], $d_l = 0.02$ cm, and $D_l = 10^{-5}$ cm^2 s^{-1}).

The current density is assumed to be relatively low to minimize cation distribution gradients within the ionomer causing thermodynamic, kinetic, and mass transport losses [7–13]. These gradients are also expected to affect ohmic losses as well as the ion exchange process because at the ionomer interface the foreign cation concentration is larger than the average value (water/ionomer boundary condition). The simplification introduced (relatively low current density) ensures that all these effects are minimized thus defining an ideal ohmic loss case useful to study the more general case and applicable to a few specific cases (uncharged contaminant uptake, gas phase contaminants). It is also assumed that the cell potential is controlled within the ohmic regime (Fig. 4). The cell polarization curve undergoes modifications as the ionomer is contaminated by the foreign cation. The behavior illustrated in Fig. 4 reproduces experimental data for different ionomer contamination levels [14]. As contamination progresses, the cell operating point moves from initial point A to point B while the trajectory remains in the ohmic regime.

Analysis of all transport processes indicate that transport only occurs by diffusion in both phases. Additionally, only liquid phase or ionomer phase diffusive transport is rate determining. A quantitative criteria was derived to determine the rate controlling step based on the following dimensionless group [15]:

$$\frac{c_i D_i d_l}{c_l D_l d_i}(5+2\alpha^{H^+}_{X+n}) << 1, \quad \text{ionomer phase diffusion control} \quad (7)$$

$$\frac{c_i D_i d_l}{c_l D_l d_i}(5+2\alpha^{H^+}_{X+n}) >> 1, \quad \text{liquid phase diffusion control} \quad (8)$$

If the diffusion coefficients are significantly different, a harmonic mean can be used [15]. Here, $c_i \gg c_l$ with $c_i = nc_{i,X^{+n}} + c_{i,H^+}$ (dilute contaminant of >10^{-7} M level to ensure ion exchange process takes place and low ionomer equivalent weight leading to an exchange site concentration of M level), $D_i \sim D_l$ (well humidified membrane with expanded pores), $d_i \ll d_l$ (25–50 μm membrane thickness in comparison to ~200 μm gas diffusion electrode thickness as depicted in Fig. 1a) and $\alpha^{H^+}_{X+n} < 1$ (for most foreign cations with the exception of $\alpha^{H^+}_{Li^+} \sim 1$). Therefore, contamination by a foreign cation is liquid phase controlled (Eq. (8) applies, Fig. 1b) because $c_i D_i d_l / c_l D_l d_i \gg 1$ by several orders of magnitude and $5 + 2\alpha^{H^+}_{X+n} > 1$.

Operating conditions are assumed to be either kept constant (stoichiometry, relative humidity, cell potential) or controlled within a narrow range (temperature, pressure [39]) to maintain a constant water balance [40] and transport parameter values (diffusion coefficient). It is also assumed that the chemical membrane degradation affecting its ion exchange capacity (loss of exchange sites) takes place with a longer time scale than cation contamination [41,42] which is favored by the use of wetter reactant streams [43]. This statement is important considering that foreign cations such as Cu^{2+}, Fe^{2+} and Fe^{3+} accelerate thermal [44] and chemical [45–49] ionomer degradation.

3. Model equations

An ion exchange model for diffusion control in the liquid phase (absence of migration and convection) was derived [15]. This model is reformulated here for the case of an ionomer sheet. Fick's first law for the proton flux is:

$$N = D_l \frac{c_{l,H^+}(d_l, t) - c_{l,H^+}(0, t)}{d_l} \quad (9)$$

The membrane proton mass balance is:

$$\frac{dc_{i,H^+}(t)V}{dt} = -AN \quad (10)$$

Reformulation of Eq. (6) in terms of concentrations leads to the following equilibrium condition at the liquid phase/ionomer phase interface:

$$c_{i,H^+}(t) = \frac{c_i \alpha^{H^+}_{X+n} c_{l,H^+}(d_l, t)}{c_l + c_{l,H^+}(d_l, t)(\alpha^{H^+}_{X+n} - 1)} \quad (11)$$

It is assumed that the ionomer is initially in a fully protonated form and that the foreign cation is much more concentrated than the proton concentration in the flow field channel water:

$$c_{l,H^+}(d_l, 0) = c_l \quad (12)$$

$$c_{l,H^+}(0, t) = 0 \quad (13)$$

Combination of Eqs. (9) to (11) and (13) leads to:

$$\frac{dc_{l,H^+}(d_l, t)}{dt}\left(\frac{1}{c_{l,H^+}(d_l, t)(c_l + (\alpha^{H^+}_{X+n} - 1)c_{l,H^+}(d_l, t))} - \frac{(\alpha^{H^+}_{X+n} - 1)c_{l,H^+}(d_l, t)}{c_{l,H^+}(d_l, t)(c_l + (\alpha^{H^+}_{X+n} - 1)c_{l,H^+}(d_l, t))^2}\right) = \frac{-D_l}{c_i d_i d_l \alpha^{H^+}_{X+n}} \quad (14)$$

The solution to Eq. (14) with the boundary condition given by Eq. (12) and re-use of Eq. (11) to replace $c_{l,H^+}(d_l, t)$ by $c_{i,H^+}(t)$ is:

$$\ln(y_{H^+}(t)) + \left(1 - \frac{1}{\alpha_{X+n}^{H^+}}\right)(1 - y_{H^+}(t)) = \frac{-c_l D_l}{c_i d_i d_l \alpha_{X+n}^{H^+}} t \quad (15)$$

The ionomer cation composition is linked to its conductivity by a linear (NH_4^+, Na^+, Ca^{2+} [23,25,28,30,31,50]) or logarithmic (NH_4^+, Na^+, Ca^{2+}, Fe^{3+} [30,31]) empirical relationship:

$$\sigma = a + b y_{H^+} \quad (16)$$

$$\ln\ \sigma = a + b y_{H^+} \quad (17)$$

Eq. (16) only applies to the absence of interactions between the proton and the foreign cation. Other relationships may be used because Eqs. (16) and (17) do not appear to fit Cu^{2+}, Ni^{2+} and Fe^{3+} data [26]. For demonstration purposes, combination of Eq. (16) with Eq. (15) leads to:

$$\ln\left(\frac{\sigma(t) - a}{b}\right) + \left(1 - \frac{1}{\alpha_{X+n}^{H^+}}\right)\left(1 - \frac{\sigma(t) - a}{b}\right) = \frac{-c_l D_l}{c_i d_i d_l \alpha_{X+n}^{H^+}} t \quad (18)$$

The cell voltage (controlled) and areal membrane resistance are, respectively:

$$E = E_c - E_a - Ri \quad (19)$$

$$R = \frac{d_i}{\sigma} \quad (20)$$

Combination of Eqs. (19) and (20) leads to (changes in thermodynamic, kinetic and mass transport losses are assumed to be negligible):

$$\frac{i(t)}{i(0)} = \frac{E_c - E_a - E}{R(t)} \frac{R(0)}{E_c - E_a - E} = \frac{R(0)}{R(t)} = \frac{d_i \sigma(t)}{\sigma(0) d_i} = \frac{\sigma(t)}{\sigma(0)} \quad (21)$$

A similar reduction is not possible for the galvanostatic case. Furthermore, Eq. (21) is consistent with prior generic models [3–6]. Combination of Eqs. (16), (18) and (21) leads to:

$$\ln\left(\frac{(i(t)/i(0))(a+b) - a}{b}\right) + \left(1 - \frac{1}{\alpha_{X+n}^{H^+}}\right)\left(1 - \frac{(i(t)/i(0))(a+b) - a}{b}\right) = \frac{-c_l D_l}{c_i d_i d_l \alpha_{X+n}^{H^+}} t \quad (22)$$

For $t \to 0$ and $t \to \infty$, Eq. (22) reduces to, respectively:

$$\frac{i(t)}{i(0)} = 1 - \frac{b}{a+b} \frac{c_l D_l}{c_i d_i d_l} t \quad (23)$$

$$\frac{i(t)}{i(0)} = \frac{a}{a+b} \quad (24)$$

For the recovery situation, it is assumed that the ionomer is initially in a fully foreign cation form and that the proton is much more concentrated than the foreign cation concentration in the flow field channel water:

$$c_{l,H^+}(d_l, 0) = 0 \quad (25)$$

$$c_{l,H^+}(0, t) = c_l \quad (26)$$

Combination of Eqs. (9) to (11) and (26) leads to:

$$\frac{dc_{l,H^+}(d_l, t)}{dt}\left(\frac{1}{(c_{l,H^+}(d_l, t) - c_l)(c_l + (\alpha_{X+n}^{H^+} - 1)c_{l,H^+}(d_l, t))} - \frac{(\alpha_{X+n}^{H^+} - 1)c_{l,H^+}(d_l, t)}{(c_{l,H^+}(d_l, t) - c_l)(c_l + (\alpha_{X+n}^{H^+} - 1)c_{l,H^+}(d_l, t))^2}\right) = \frac{-D_l}{c_i d_i d_l \alpha_{X+n}^{H^+}} \quad (27)$$

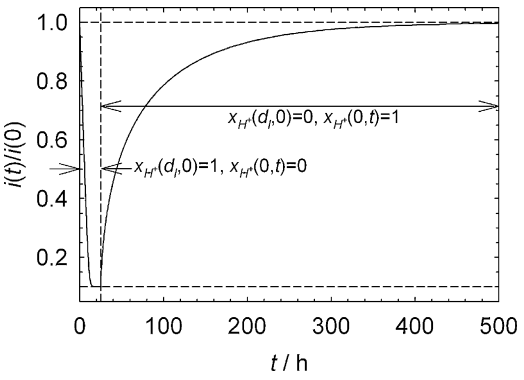

Fig. 5. Effect of contamination by a foreign cation and subsequent recovery on the cell normalized current density (Eqs. (22) and (29)). $a = 0.01\ \Omega^{-1}\ cm^{-1}$, $b = 0.09\ \Omega^{-1}\ cm^{-1}$, $\alpha_{X+n}^{H^+} = 0.1$, $c_i d_i d_l / c_l D_l = 10$ h.

The solution to Eq. (27) with the boundary condition given by Eq. (25) and re-use of Eq. (11) to replace $c_{l,H^+}(d_l, t)$ by $c_{i,H^+}(t)$ is:

$$\ln(1 - y_{H^+}(t)) + \left(1 - \alpha_{X+n}^{H^+}\right) y_{H^+}(t) = \frac{-c_l D_l \alpha_{X+n}^{H^+}}{c_i d_i d_l} t \quad (28)$$

Combination of Eqs. (16) and (21) with Eq. (28) leads to:

$$\ln\left(1 - \frac{(i(t)/i(0))(a+b) - a}{b}\right) + (1 - \alpha_{X+n}^{H^+})\left(\frac{(i(t)/i(0))(a+b) - a}{b}\right) = \frac{-c_l D_l \alpha_{X+n}^{H^+}}{c_i d_i d_l} t \quad (29)$$

For $t \to 0$ and $t \to \infty$, Eq. (29) reduces to, respectively:

$$\frac{i(t)}{i(0)} = \frac{a}{a+b} + \frac{b}{a+b} \frac{c_l D_l}{c_i d_i d_l} t \quad (30)$$

$$\frac{i(t)}{i(0)} = 1 \quad (31)$$

Fig. 5 illustrates Eqs. (22) and (29) for arbitrary parameter values. It is observed that recovery is significantly slower than contamination, which is consistent with a preferred foreign cation in the ionomer (Figs. 2 and 3), but proceeds to completion with the proton form re-established because $x_{X+n} \approx 0$. Eqs. (22) and (29) time scales differ by a $(\alpha_{X+n}^{H^+})^2$ factor resulting in a 1/100 ratio in Fig. 5 ($\alpha_{X+n}^{H^+} = 0.1$). Steady states are indicated and given by Eqs. (24) and (31) whereas initial linear regimes are given by Eqs. (23) and (30).

4. Results and discussion

4.1. Model validation

Two problems complicate model validation. In the first instance, ohmic loss measurements do not represent the actual ionomer conductivity [11]. During steady state operation, the inactive foreign cation flux is equal to zero. However, ohmic measurements performed with alternating currents or potentials affect all cations present in the ionomer. Therefore, the resulting measurement values include a contribution from foreign cations. If direct current or potential methods are used instead to ensure establishment of a steady state foreign cation concentration profile (zero flux), proton depletion occurs at one of the electrodes leading to thermodynamic, kinetic and mass transport losses thus complicating separation of the ionomer ohmic loss contribution.

The absence of complete and extensive cell performance data sets constitutes the second validation problem. Only few data sets are available in the form of current, potential or resistance time

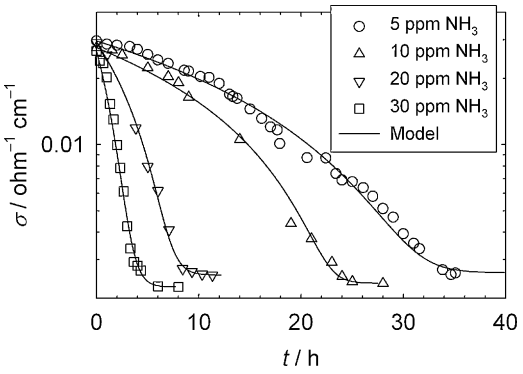

Fig. 6. Effect of NH_3 contamination on transient membrane conductivity. Model curves result from fitting to Eq. (18). Parameter values are listed in Table 2.

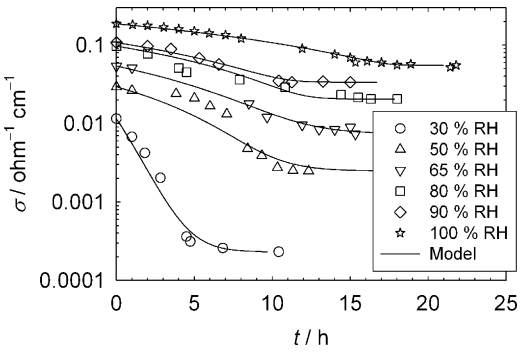

Fig. 7. Effect of gas phase relative humidity on transient membrane conductivity. Model curves result from fitting to Eq. (18). Parameter values are listed in Table 2.

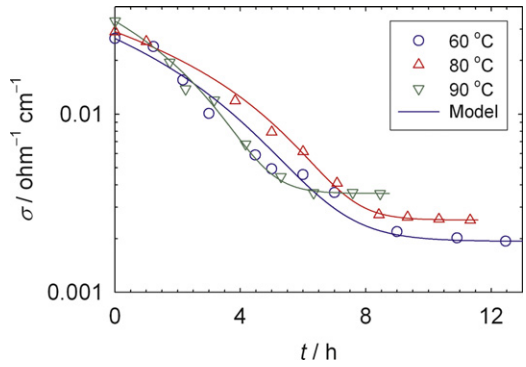

Fig. 8. Effect of temperature on transient membrane conductivity. Model curves result from fitting to Eq. (18). Parameter values are listed in Table 2.

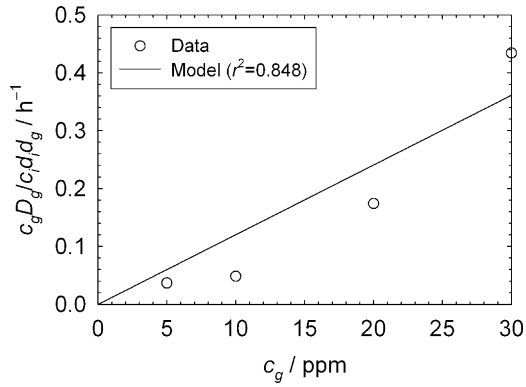

Fig. 9. Model parameter $c_gD_g/c_id_id_g$ (Table 2) as a function of c_g. A significant linear correlation is also displayed.

series for a restricted range of foreign cations (NH_3/NH_4^+, Na^+, Co^{2+}, Fe^{3+}, Al^{3+}, Pt (unspecified valence) [51–57]). More specifically, data sets are generally not obtained under potentiostatic control or until steady states are achieved (including recovery). Therefore, the model limit of applicability cannot be quantitatively defined because relevant experimental data sets are not available and, a comparison between model predictions and experimental data, cannot be completed. It is noted that cell performance losses are significant as demonstrated by NaCl poisoning leading to a current density loss of 33% at 0.6 V [55]. For ammonia (NH_4^+), cell performance losses were concentration dependent and amounted to current density decreases at 0.5 V of 25 and 50% for respectively 13 and 130 ppm [55].

Recently, poisoning experiments were performed with NH_3, an important hydrogen fuel contaminant [58], and a membrane rather than a complete fuel cell membrane/electrode assembly [30,50,59]. Ohmic measurements were completed in absence of reactants and with alternating currents or potentials (uniform concentration profiles). Results are thus reflective of the ionomer state (composition is the focus rather than a measurement of the ohmic loss during fuel cell operation). These data sets offer an opportunity to partly test the present ohmic loss contamination model without interference from other loss mechanisms. However, recovery cannot be investigated in this manner unless liquid water is circulated and contacts the membrane.

Figs. 6–8 illustrate the effects of NH_3 concentration, relative humidity (RH) and temperature on membrane conductivity as a function of time. Eq. (18) with 4 parameters (a, b, $\alpha_{X^{+n}}^{H^+}$, $c_id_id_l/c_lD_l$) was used and fitted to experimental data. Parameters a and b are already known and are respectively derived from the initial ($y_{X^{+n}} = 0$, $\sigma = a + b$) and steady state ($y_{X^{+n}} = 1$, $\sigma = a$) conductivity values. The two other parameters were obtained by least square fitting (SigmaPlot version 10, Marquardt–Levenberg algorithm). Table 2 lists all parameter values determined using Figs. 6–8 data. It is noted that correlation coefficients generally exceed 0.97 indicating that the model accurately reproduces all data sets. Clearly, NH_3 diffusion in the gas phase does not appear to correspond to the model's physical picture of a foreign cation moving into water (Fig. 1a). This apparent discrepancy is rationalized by pointing out that the NH_3 species still moves predominantly by diffusion in the gas phase boundary layer (absence of convection and migration). Thus, in Eqs. (7) and (8), liquid phase values can be replaced by their gas phase equivalents. Here, $c_i \gg c_g$ and $d_i < d_g$, but $D_i \ll D_g$. However, contamination by NH_3 is gas phase controlled (Eq. (8) applies) because $c_iD_id_g/c_gD_gd_i \gg 1$ and $5 + 2\alpha_{X^{+n}}^{H^+} > 1$. At the gas phase/ionomer interface, the following fast reaction [60] ensures that a NH_4^+ concentration is established effectively creating an effect similar to ion exchange (a foreign cation penetrates the ionomer whereas the proton is removed from the ionomer, Fig. 1a):

$$NH_3 + H^+ \rightarrow NH_4^+ \quad (32)$$

The reverse reaction is not considered because recovery was not observed in the absence of ammonia even after a period of one day [30]. A final confirmation is provided by plotting the $c_gD_g/c_id_id_g$ parameter (Table 2) as a function of c_g (Fig. 9). As expected, a significant linear correlation is obtained. Eq. (32) also takes place in liquid water which means that in an application (in the presence of a membrane/electrode assembly rather than a membrane), the ammonia species behavior is closer to a foreign cation (ammonium).

4.2. Model parameters determination

All Eq. (22) parameters (a, b, $\alpha_{X^{+n}}^{H^+}$, $c_id_id_l/c_lD_l$) are easily determined if the initial ionomer proton form conductivity is known (Eq.

Table 1
Ion exchange isotherm parameters[a] summary (Fig. 3).

Foreign cation	$\alpha_{X+n}^{H^+}$	r^2
NH_4^+	0.427	0.988
Na^+	1.25	0.998
Ca^{2+}	0.0933	0.981
Fe^{3+}	0.00106	0.965

[a] Nafion 417 data [31].

(16)):

$$Est_1 = a + b \tag{33}$$

The limiting dimensionless current density during contamination (Eq. (24)) provides the experimental value required to isolate a and b parameters:

$$Est_2 = \frac{a}{a+b} \tag{34}$$

Eqs. (33) and (34) leads to:

$$a = Est_1 Est_2 \tag{35}$$

$$b = Est_1(1 - Est_2) \tag{36}$$

Eqs. (23) and (30) have a similar slope providing independent estimates for $c_i d_i d_l / c_l D_l$ (estimates can be used to verify model consistency). Eqs. (33) and (36) lead to:

$$Est_3 = \frac{b}{a+b}\frac{c_l D_l}{c_i d_i d_l} = (1 - Est_2)\frac{c_l D_l}{c_i d_i d_l} \tag{37}$$

Rearrangement of Eq. (37) leads to:

$$\frac{c_i d_i d_l}{c_l D_l} = \frac{1 - Est_2}{Est_3} \tag{38}$$

The time required for the dimensionless current to decrease to a value equal to half the difference between initial and steady state values $t_{0.5}$ (contamination) represents the last estimate:

$$Est_4 = t_{0.5} \tag{39}$$

The corresponding dimensionless current is using Eq. (24):

$$\frac{i(t_{0.5})}{i(0)} = \frac{i(0) - i(\infty)}{2i(0)} = \frac{1}{2}\left(1 - \frac{a}{a+b}\right) \tag{40}$$

Replacement of Eq. (40) in Eq. (22) and use of Eqs. (35), (36) and (38) leads to:

$$\alpha_{X+n}^{H^+} = \frac{\frac{1}{2} + \frac{Est_2 - Est_3 Est_4}{1 - Est_2}}{\ln\left(\frac{1}{2} - \frac{Est_2}{1 - Est_2}\right) + \frac{1}{2} + \frac{Est_2}{1 - Est_2}} \tag{41}$$

The equivalent derivation for the recovery case using Eqs. (29) leads to:

$$\alpha_{X+n}^{H^+} = \frac{\ln\left(\frac{1}{2} + \frac{Est_2}{1 - Est_2}\right) + \frac{1}{2} - \frac{Est_2}{1 - Est_2}}{\frac{1}{2} - \frac{Est_2 + Est_3 Est_4}{1 - Est_2}} \tag{42}$$

Eq. (42) provides a second estimate that can be used to verify model consistency.

4.3. Contamination mechanism

It was indicated in Section 4.1 that validation data sets are incomplete. However, the information available supports the present model. For instance, partial or complete performance recovery was noted [51,53]. More specifically, experimental data for Fe^{3+}, representing a worse case scenario with $\alpha_{Fe^{3+}}^{H^+} \ll 1$ (higher charge cations are strongly preferred by the ionomer as shown in Fig. 3 and Table 1 [26,31]), are reexamined. A membrane in the Fe^{3+} form was used to make a membrane/electrode assembly that was conditioned with wet reactant streams [14]. The cell voltage increased from 0 V until cell operation was possible demonstrating ion exchange by protons from water dissociation (Eq. (1)). A more complete model validation requires additional data obtained under specific operating conditions (cell voltage control, sequential contamination and recovery transients obtained until steady states are reached, data obtained for relevant ranges of foreign cation concentration and cell potential, etc.).

A model library is systematically and incrementally developed. As the current density is increased, leading performance losses change from kinetic to ohmic and mass transport losses (Fig. 4). The development of this library is following a similar path. Initially, contaminants leading to kinetic losses were examined [4,6] followed by ohmic losses (this work). Contaminants creating mass transport losses will be examined after the library is populated with known or envisaged contaminant mechanisms leading to ohmic losses. Some of the existing models will likely need a revision including ionomer contamination by a foreign cation to take account of thermodynamic, kinetic and mass transport losses associated with cations redistribution within the ionomer (this work). This approach was selected to manage the significant amount of work necessary to cover existing ([4,6], this work) and envisaged cases by separating it into more easily tackled parts. This approach is also expected to facilitate the study of contaminant mixtures and the simultaneous presence of several types of performance losses.

Table 3 summarizes the features of the present model as well as other model versions derived for other cases using a similar approach. Most of these cases are representative of known contamination kinetics. The first 4 cases are related to catalyst contamination and within this category, 3 cases pertain to electroactive contaminants: the contaminant X adsorbs and reacts leading to a product P_2 (such as CO on Pt above 0.5 V vs. RHE or, NO on Pt below 0.6 V vs. RHE or above 0.9 V vs. RHE) with a surface reaction or product desorption rate determining step (rds), the contaminant X adsorbs but only reacts at segregated sites leading to an irreversibly adsorbed product P_2 (such as SO_2 or H_2S on Pt between 0.05 and 1 V vs. RHE). The 4th case related to catalyst contamination represents an electroinactive contaminant (such as CO on Pt at <0.5 V vs. RHE or NO on Pt between 0.6 and 0.9 V vs. RHE). The 5th case pertains to the present model and expands for the first time the model library into ionomer contamination kinetics (a significant and important step). The current density i qualitatively shows a similar transient behavior for all cases due to the overwhelming effect of the much more concentrated reactant species with the exception of an electroactive contaminant that leads to an irreversibly adsorbed product P_2. Thus, a distinction between all cases is not possible. By contrast, experiments performed without a reactant lead to the contaminant related current density i_X or i_{X+n} and different transients for each case with the exception of the present membrane contamination model. Contamination mechanism identification with minimal testing requirements is thus significantly facilitated. Separation between membrane and catalyst (X electroinactive) contamination cases is conceivably possible using additional cell resistance measurements [51]. An accurate measurement is not necessary (Section 4.1) but rather only an indication that the membrane resistance is affected to discriminate between cases. As already indicated in Section 2, cation distribution gradients within the ionomer prevent accurate membrane resistance measurements [7–13,61,62].

4.4. Model predictions

It was reported that small amounts of foreign cations, such as Na^+, Cu^{2+}, Ni^{2+}, Fe^{3+}, significantly impact the membrane conductivity at the ~10–310 ppm level [63–65]. Therefore, there is a need to prevent the gradual replacement of ionomer protons by foreign cations because procedures to maintain such a low contamina-

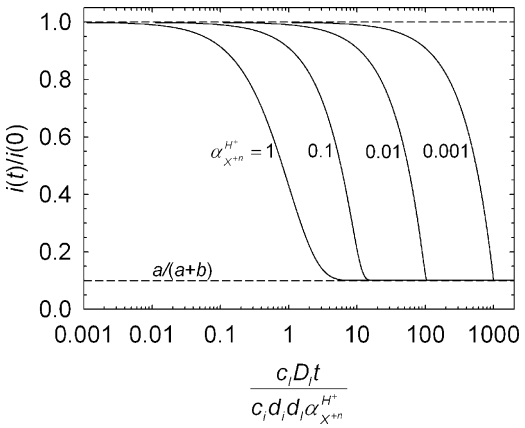

Fig. 10. Effect of the separation factor on dimensionless contamination transients. $a = 0.01\ \Omega^{-1}\ cm^{-1}$ and $b = 0.09\ \Omega^{-1}\ cm^{-1}$.

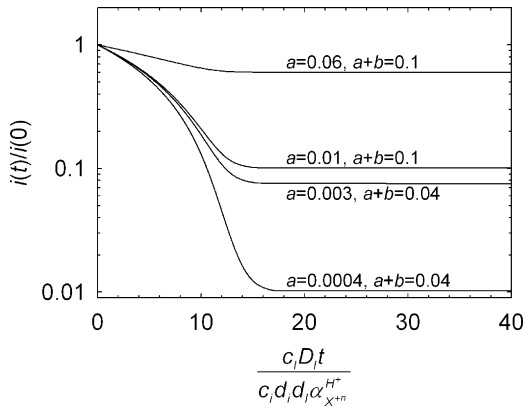

Fig. 11. Effect of the ionomer conductivity on dimensionless contamination transients. a and b units are $\Omega^{-1}\ cm^{-1}$, $\alpha^{H^+}_{X^{+n}} = 0.1$.

tion level are still under development. The ionomer contamination model suggests operating conditions and design based mitigation strategies. Eq. (22) indicates that a decrease in temperature (D_l) and a relative decrease in foreign cation concentration (c_l) slow the contamination process. Conversely, an increase in temperature and a relative increase in proton concentration (relative decrease in foreign cation concentration) accelerate the recovery process (Eq. (29)). From a design standpoint, strategies are more limited because practical ionomer choices (c_i) and their thickness (d_i) are restricted by other considerations. For instance, lower equivalent weights and thicker materials are respectively more prone to water uptake (induced mechanical stresses) and larger ohmic losses. Similar considerations apply to the gas diffusion layer (d_l) with a negative impact on volumetric power density and material cost.

Eqs. (22) and (29) indicate that a, b and $\alpha^{H^+}_{X^{+n}}$ parameters influence transients in several ways because they appear multiple times. Thus the overall effect is not easily discernible. As a result, the effect of all these parameters on both contamination and recovery transients were computed for a relevant range of parameter values. Although relative humidity is not specifically included in the model derivation, model predictions based on ionomer conductivities resulting from exposure to different relative humidity environments are expected to hold as long as liquid water is present in the flow field channel/gas diffusion electrode and contacts the ionomer because the physical description of the process still holds (Fig. 1a). Fig. 10 illustrates the effect of $\alpha^{H^+}_{X^{+n}}$ which shows that a smaller value delays contamination. This is at first sight counterintuitive because lower separation factor values are associated with higher valence foreign cations which are strongly preferred by the ionomer (Fig. 3). However, the time scale $c_i d_i d_l \alpha^{H^+}_{X^{+n}} / c_l D_l$ (Eq. (22)) is in effect largely reduced as expected thus creating a larger dimensionless time. It is also noted that the approach to a steady state value is sharper as the separation factor value decreases. Fig. 11 displays the effect of both relative humidity and foreign cation. The top 2 curves correspond to an ionomer exposed to a saturated stream ($a + b = 0.1\ \Omega^{-1}\ cm^{-1}$ [31]) whereas the bottom 2 curves correspond to an ionomer exposed to a 50% relative humidity stream ($a + b = 0.04\ \Omega^{-1}\ cm^{-1}$ [31]). For the same relative humidity, each curve pair shows the range of expected ionomer conductivity in the foreign cation form ($a = 0.01$ for Na^+, Ca^{2+}, Fe^{3+} to 0.06 for NH_4^+ and 0.0004 for Na^+, Ca^{2+}, Fe^{3+} to 0.003 for NH_4^+ $\Omega^{-1}\ cm^{-1}$ [31]). It is observed that both relative humidity and foreign cation do not influence the contamination process as expected because the time scale $c_i d_i d_l \alpha^{H^+}_{X^{+n}} / c_l D_l$ is not dependent on these variables. It is also observed that relative humidity has a large impact on the dimensionless current density steady state value. Therefore, ionomer contamination by foreign cations is relatively more severe

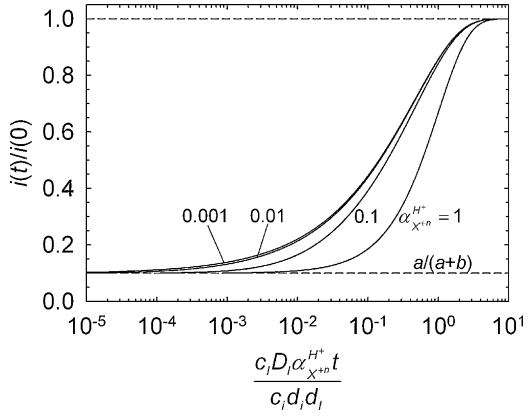

Fig. 12. Effect of the separation factor on dimensionless recovery transients. $a = 0.01\ \Omega^{-1}\ cm^{-1}$ and $b = 0.09\ \Omega^{-1}\ cm^{-1}$.

under low relative humidity conditions and does not support the development of ionomers able to operate under such conditions [66]. Fig. 12 shows the effect of $\alpha^{H^+}_{X^{+n}}$ on recovery transients demonstrating that larger values delay recovery to a proton form. This counter-intuitive result, a small separation factor is expected to facilitate ion exchange by protons, is explained by considering Eq. (29) time scale $c_i d_i d_l / c_l D_l \alpha^{H^+}_{X^{+n}}$. A larger separation factor leads to a smaller time scale and thus to a larger dimensionless time value. The approach to a steady state value remains smooth for all separation factor values contrasting with Fig. 10 results. Fig. 13 depicts the effect of both relative humidity and foreign cation in a similar

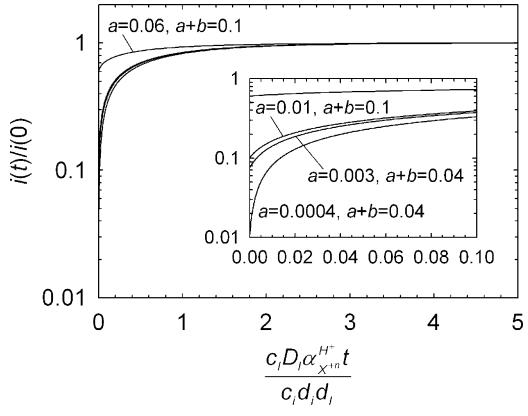

Fig. 13. Effect of the ionomer conductivity on dimensionless recovery transients. a and b units are $\Omega^{-1}\ cm^{-1}$, $\alpha^{H^+}_{X^{+n}} = 0.1$.

Table 2
Contamination model parameters summary.

Validation data		a (Ω^{-1} cm^{-1})	b (Ω^{-1} cm^{-1})	$\alpha^{H^+}_{X^{+n}}$	$c_i d_i d_l / c_l D_l$/h	r^2
Fig. 6	5 ppm NH_3	0.00261	0.0270	0.0617	27.2	0.990
	10 ppm NH_3	0.00234	0.0253	0.0394	20.7	0.994
	20 ppm NH_3	0.00255	0.0265	0.131	5.75	0.997
	30 ppm NH_3	0.00225	0.0244	0.281	2.30	0.983
Fig. 7	30% RH	0.00023	0.0113	0.752	1.44	0.973
	50% RH	0.00248	0.0269	0.217	7.08	0.856
	65% RH	0.00737	0.0465	0.210	8.87	0.974
	80% RH	0.0205	0.0763	0.0761	10.3	0.916
	90% RH	0.0337	0.0739	0.0805	9.46	0.969
	100% RH	0.0552	0.131	0.0286	16.3	0.990
Fig. 8	60 °C	0.00193	0.0247	0.211	4.91	0.971
	80 °C	0.00254	0.0265	0.108	6.03	0.993
	90 °C	0.00358	0.0297	0.157	3.72	0.973

Table 3
Summary of model behavior for different fuel cell contamination kinetics.

Measured variable for step changes in contaminant concentration				i ($c_R \neq 0$)	i_X or $i_{X^{+n}}$ ($c_R = 0$)
Catalyst contamination kinetics	X electroactive leading to a product P_2	X reaction rds [4]	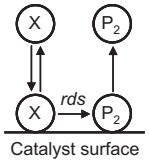	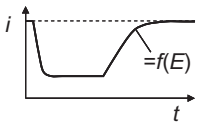	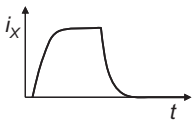
		P_2 desorption rds [4]	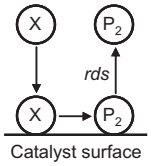	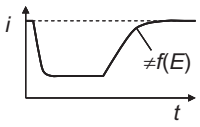	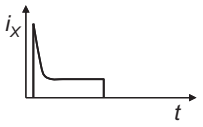
		Irreversible P_2 adsorption [6]	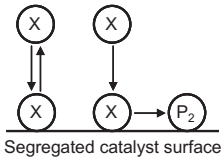	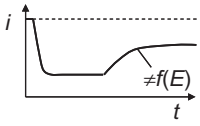	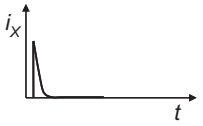
	X electroinactive [4]		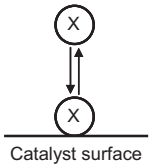	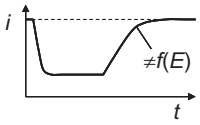	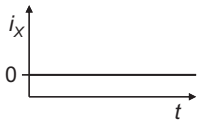
Membrane contamination kinetics	X^{+n} electroinactive (this work)		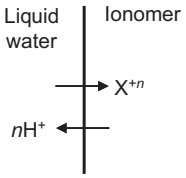	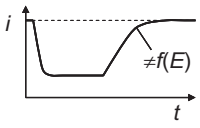	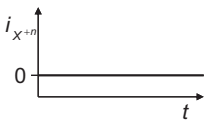

fashion as Fig. 11. It is observed that in each case full recovery is achieved with a time scale independent of relative humidity and foreign cation despite a large variation in initial dimensionless current density.

Recently, low levels of foreign divalent or trivalent cations were proposed to mitigate ionomer degradation (radical scavengers) [67–69]. Experimental data show that these cations are retained by the ionomer for a period of time exceeding 6000 h [67,69]. The present model properly predicts the long residence time of a higher valence cation in an ionomer. For example, Fig. 12 shows a dimensionless time of about 4 for recovery in the presence of a trivalent cation ($\alpha^{H^+}_{X^{+n}} \sim 0.001$ in Table 1). The combination of this value with a $\sim$0.001 separation factor for Fe^{3+} (Table 1) and a value of $c_i d_i d_l / c_l D_l$ of $\sim$1–30 h (Table 2) leads to a recovery time varying from 4000 to 120,000 h which is in good agreement with the observed 6000+ h time scale.

5. Conclusion

A PEMFC contamination model was derived for the case of a foreign cation displacing the ionomer proton. The model was derived by taking account of only key processes to obtain analytical solutions and facilitate a widespread implementation. Model validation indicates that the simplified approach derivation is

accurate and represents a benchmark for a more complicated model that includes migration effects. Additional fuel cell validation data obtained at low and high current densities (cell voltage control, sequential contamination and recovery transients obtained until steady states are reached) are desirable including the effect of foreign cation composition and concentration, etc. This is especially important considering many contaminants and their effects have not yet been identified or defined including cations that originate from system materials or are produced from reactions involving airborne species [2]. These cation sources are currently under investigation within the United States Department of Energy program. Other model extensions need to be considered including foreign cations that are reducible and that impact oxygen reduction kinetics (Cu^{2+} and Co^{2+} [12], Ru^{+n} [70]). The effect of the foreign cation uneven distribution within the ionomer affecting thermodynamic, kinetic and mass transport losses also need to be taken into account [7–13]. From that standpoint, the negative impact of foreign cations in the ionomer on reactant permeability [71–75] has not yet been considered. Model predictions suggest the use of mitigation strategies and a reconsideration of low water requirement ionomer development programs.

Acknowledgements

The author is indebted to the United States Department of Energy, Energy Efficiency and Renewable Energy for funding (National Renewable Energy Laboratory sub-contract ZGB-0-99180-01). The author also thanks Kitiya Hongsirikarn for providing data files used for model validation (Figs. 3 and 6–8).

References

[1] J. Garche, C.K. Dyer, P. Moseley, Z. Ogumi, D. Rand, B. Scrosati (Eds.), Encyclopedia of Electrochemical Power Sources, Elsevier, Amsterdam, 2009.
[2] J. St-Pierre, in: F.N. Büchi, M. Inaba, T.J. Schmidt (Eds.), Polymer Electrolyte Fuel Cell Durability, Springer, New York, 2009, p. 289.
[3] J. St-Pierre, N. Jia, R. Rahmani, J. Electrochem. Soc. 155 (2008) B315.
[4] J. St-Pierre, J. Electrochem. Soc. 156 (2009) B291.
[5] J. St-Pierre, Electrochim. Acta 55 (2010) 4208.
[6] J. St-Pierre, J. Power Sources 195 (2010) 6379.
[7] T. Okada, J. Electroanal. Chem. 465 (1999) 1.
[8] T. Okada, J. Electroanal. Chem. 465 (1999) 18.
[9] F. Chen, Y.-G. Su, C.-Y. Soong, W.-M. Yan, H.-S. Chu, J. Electroanal. Chem. 566 (2004) 85.
[10] A.Z. Weber, C. Delacourt, Fuel Cells 8 (2008) 459.
[11] B.L. Kienitz, H. Baskaran, T.A. Zawodzinski Jr., Electrochim. Acta 54 (2009) 1671.
[12] T.A. Greszler, T.E. Moylan, H.A. Gasteiger, in: W. Vielstich, H. Yokokawa, H.A. Gasteiger (Eds.), Handbook of Fuel Cells – Fundamentals, Technology and Applications, vol. 6, John Wiley and Sons, 2009, p. 728.
[13] M.F. Serincan, U. Pasaogullari, T. Molter, Int. J. Hydrogen Energy 35 (2010) 5539.
[14] J. St-Pierre, D.P. Wilkinson, S. Knights, M.L. Bos, J. New Mater. Electrochem. Syst. 3 (2000) 99.
[15] F. Helfferich, Ion Exchange, Dover Publications, New York, 1995.
[16] F.Y. Zhang, X.G. Yang, C.Y. Wang, J. Electrochem. Soc. 153 (2006) A225.
[17] A. Bazylak, D. Sinton, N. Djilali, J. Power Sources 176 (2008) 240.
[18] A. Lehmani, P. Turq, M. Périé, J. Périé, J.-P. Simonin, J. Electroanal. Chem. 428 (1997) 81.
[19] K. Matsuoka, S. Sakamoto, K. Nakato, A. Hamada, Y. Itoh, J. Power Sources 179 (2008) 560.
[20] J. McBreen, J. Electrochem. Soc. 132 (1985) 1112.
[21] W.-Y. Tu, W.-J. Liu, C.-S. Cha, B.-L. Wu, Electrochim. Acta 43 (1998) 3731.
[22] W.-J. Liu, B.-L. Wu, C.-S. Cha, J. Electroanal. Chem. 476 (1999) 101.
[23] T. Okada, N. Nakamura, M. Yuasa, I. Sekine, J. Electrochem. Soc. 144 (1997) 2744.
[24] S. Logette, C. Eysseric, G. Pourcelly, A. Lindheimer, C. Gavach, J. Membr. Sci. 144 (1998) 259.
[25] T. Okada, S. Møller-Holst, O. Gorseth, S. Kjelstrup, J. Electroanal. Chem. 442 (1998) 137.
[26] T. Okada, Y. Ayato, M. Yuasa, I. Sekine, J. Phys. Chem. B 103 (1999) 3315.
[27] T. Okada, H. Satou, M. Okuno, M. Yuasa, J. Phys. Chem. B 106 (2002) 1267.
[28] R. Halseid, P.J.S. Vie, R. Tunold, J. Electrochem. Soc. 151 (2004) A381.
[29] J. Ramkumar, T. Mukherjee, Sep. Purif. Technol. 54 (2007) 61.
[30] K. Hongsirikarn, J.G. Goodwin Jr., S. Greenway, S. Creager, J. Power Sources 195 (2010) 30.
[31] K. Hongsirikarn, J.G. Goodwin Jr., S. Greenway, S. Creager, J. Power Sources 195 (2010) 7213.
[32] H. Miyoshi, M. Yamagami, M. Chubachi, T. Kataoka, J. Chem. Eng. Data 39 (1994) 595.
[33] H. Meng, C.-Y. Wang, J. Electrochem. Soc. 151 (2004) A358.
[34] P.C. Sui, N. Djilali, J. Power Sources 161 (2006) 294.
[35] A.J. Bard, L.R. Faulkner, Electrochemical Methods – Fundamentals and Applications, 2nd ed., John Wiley and Sons, 2001, pp. 63 and 143.
[36] L. Axe, P.R. Anderson, in: E. Jenne (Ed.), Adsorption of Metals by Geomedia: Variables, Mechanisms, and Model Applications, Academic Press, New York, 1998, p. 193.
[37] H.S. Fogler, Elements of Chemical Reaction Engineering, 4th ed., Prentice Hall, Upper Saddle River, NJ, 2006, p. 958.
[38] A. Esposito, C. Pianese, Y.G. Guezennec, J. Power Sources 195 (2010) 4149.
[39] D.P. Wilkinson, J. St-Pierre, J. Power Sources 113 (2003) 101.
[40] J. St-Pierre, J. Roberts, K. Colbow, S. Campbell, A. Nelson, J. New Mater. Electrochem. Syst. 8 (2005) 163.
[41] R. Borup, J. Meyers, B. Pivovar, Y.S. Kim, R. Mukundan, N. Garland, D. Myers, M. Wilson, F. Garzon, D. Wood, P. Zelenay, K. More, K. Stroh, T. Zawodzinski, J. Boncella, J.E. McGrath, M. Inaba, K. Miyatake, M. Hori, K. Ota, Z. Ogumi, S. Miyata, A. Nishikata, Z. Siroma, Y. Uchimoto, K. Yasuda, K.-I. Kimijima, N. Iwashita, Chem. Rev. 107 (2007) 3904.
[42] A. Kabasawa, J. Saito, K. Miyatake, H. Uchida, M. Watanabe, Electrochim. Acta 54 (2009) 2754.
[43] S.D. Knights, K.M. Colbow, J. St-Pierre, D.P. Wilkinson, J. Power Sources 127 (2004) 127.
[44] C. Bas, L. Reymond, A.-S. Danérol, N.D. Albérola, E. Rossinot, L. Flandin, J. Polym. Sci. B 47 (2009) 1381.
[45] A. Pozio, R.F. Silva, M. De Francesco, L. Giorgi, Electrochim. Acta 48 (2003) 1543.
[46] M.K. Kadirov, A. Bosnjakovic, S. Schlick, J. Phys. Chem. B 109 (2005) 7664.
[47] M. Aoki, H. Uchida, M. Watanabe, Electrochem. Commun. 8 (2006) 1509.
[48] M. Inaba, T. Kinumoto, M. Kiriake, R. Umebayashi, A. Tasaka, Z. Ogumi, Electrochim. Acta 51 (2006) 5746.
[49] T. Kinumoto, M. Inaba, Y. Nakayama, K. Ogata, R. Umebayashi, A. Tasaka, Y. Iriyama, T. Abe, Z. Ogumi, J. Power Sources 158 (2006) 1222.
[50] K. Hongsirikarn, X. Mo, J.G. Goodwin Jr., J. Power Sources 195 (2010) 3416.
[51] F.A. Uribe, S. Gottesfeld, T.A. Zawodzinski Jr., J. Electrochem. Soc. 149 (2002) A293.
[52] P. Yu, M. Pemberton, P. Plasse, J. Power Sources 144 (2005) 11.
[53] R. Halseid, P.J.S. Vie, R. Tunold, J. Power Sources 154 (2006) 343.
[54] M.S. Mikkola, T. Rockward, F.A. Uribe, B.S. Pivovar, Fuel Cells 7 (2007) 153.
[55] B.S. Pivovar, B. Kienitz, T. Rockward, F.A. Uribe, F.H. Garzon, in: W. Vielstich, H. Yokokawa, H.A. Gasteiger (Eds.), Handbook of Fuel Cells – Fundamentals, Technology and Applications, vol. 6, John Wiley and Sons, 2009, p. 718.
[56] H. Li, K. Tsay, H. Wang, S. Wu, J. Zhang, N. Jia, S. Wessel, R. Abouatallah, N. Joos, J. Schrooten, Electrochim. Acta 55 (2010) 2622.
[57] H. Li, K. Tsay, H. Wang, J. Shen, S. Wu, J. Zhang, N. Jia, S. Wessel, R. Abouatallah, N. Joos, J. Schrooten, J. Power Sources 195 (2010) 8089.
[58] ISO/CD 14687-2, 2009.
[59] K. Hongsirikarn, X. Mo, Z. Liu, J.G. Goodwin Jr., J. Power Sources 195 (2010) 5493.
[60] J.J. Renard, S.E. Calidonna, M.V. Henley, J. Hazard. Mater. 108 (2004) 29.
[61] R.A. Rozendal, H.V.M. Hamelers, C.J.N. Buisman, Environ. Sci. Technol. 40 (2006) 5206.
[62] X. Jie, Z.-G. Shao, J. Hou, G. Sun, B. Yi, Electrochim. Acta 55 (2010) 4783.
[63] M.J. Kelly, G. Fafilek, J.O. Besenhard, H. Kronberger, G.E. Nauer, J. Power Sources 145 (2005) 249.
[64] M.J. Kelly, B. Egger, G. Fafilek, J.O. Besenhard, H. Kronberger, G.E. Nauer, Solid State Ionics 176 (2005) 2111.
[65] J.C. Bendert, D.D. Papadias, D.J. Myers, J. Electrochem. Soc. 157 (2010) B1486.
[66] N.L. Garland, J.P. Kopasz, J. Power Sources 172 (2007) 94.
[67] E. Endoh, Electrochem. Soc. Trans. 16 (2) (2008) 1229.
[68] F.D. Coms, H. Liu, J.E. Owejan, Electrochem. Soc. Trans. 16 (2) (2008) 1735.
[69] E. Endoh, Electrochem. Soc. Trans. 25 (35) (2010) 293.
[70] L. Gancs, B.N. Hult, N. Hakim, S. Mukerjee, Electrochem. Solid-State Lett. 10 (2007) B150.
[71] T. Okada, J. Dale, Y. Ayato, O.A. Asbjørnsen, M. Yuasa, I. Sekine, Langmuir 15 (1999) 8490.
[72] T. Okada, Y. Ayato, J. Dale, M. Yuasa, I. Sekine, O.A. Asbjørnsen, Phys. Chem. Chem. Phys. 2 (2000) 3255.
[73] T. Okada, Y. Ayato, H. Satou, M. Yuasa, I. Sekine, J. Phys. Chem. B 105 (2001) 6980.
[74] T. Okada, H. Satou, M. Yuasa, Langmuir 19 (2003) 2325.
[75] H.F.M. Mohamed, Y. Kobayashi, C.S. Kuroda, A. Ohira, J. Phys. Chem. B 113 (2009) 2247.